3D Printing of Liquid Crystalline Hydroxypropyl Cellulose—toward Tunable and Sustainable **Volumetric Photonic Structures**

Chun Lam Clement Chan, Iek Man Lei, Gea T. van de Kerkhof, Richard M. Parker, Kieran D. Richards, Rachel C. Evans, Yan Yan Shery Huang, and Silvia Vignolini*

Additive manufacturing is becoming increasingly important as a flexible technique for a wide range of products, with applications in the transportation, health, and food sectors. However, to develop additional functionality it is important to simultaneously control structuring across multiple length scales. In 3D printing, this can be achieved by employing inks with intrinsic hierarchical order. Liquid crystalline systems represent such a class of self-organizing materials; however, to date they are only used to create filaments with nematic alignment along the extrusion direction. In this study, cholesteric hydroxypropyl cellulose (HPC) is combined with in situ photo-crosslinking to produce filaments with an internal helicoidal nanoarchitecture, enabling the direct ink writing of solid, volumetric objects with structural color. The iridescent color can be tuned across the visible spectrum by exploiting either the lyotropic or thermotropic behavior of HPC during the crosslinking step, allowing objects with different colors to be printed from the same feedstock. Furthermore, by examining the microstructure after extrusion, the role of shear within the nozzle is revealed and a mechanism proposed based on rheological measurements simulating the nozzle extrusion. Finally, by using only a sustainable biopolymer and water, a pathway toward environmentally friendly 3D printing is revealed.

C. L. C. Chan, G. T. van de Kerkhof, R. M. Parker, S. Vignolini Yusuf Hamied Department of Chemistry University of Cambridge Lensfield Road, Cambridge CB2 1EW, UK E-mail: sv319@cam.ac.uk I. M. Lei, Y. Y. S. Huang Department of Engineering University of Cambridge Trumpington Street, Cambridge CB2 1PZ, UK K. D. Richards, R. C. Evans Department of Materials Science and Metallurgy University of Cambridge 27 Charles Babbage Road, Cambridge CB3 0FS, UK

The ORCID identification number(s) for the author(s) of this article can be found under https://doi.org/10.1002/adfm.202108566.

© 2022 The Authors. Advanced Functional Materials published by Wiley-VCH GmbH. This is an open access article under the terms of the Creative Commons Attribution License, which permits use, distribution and reproduction in any medium, provided the original work is properly cited.

DOI: 10.1002/adfm.202108566

1. Introduction

For the design of complex hierarchical materials, the ability to simultaneously control structuring across multiple length scales is key to unlocking novel functionalities. This is achieved in additive manufacturing systems by combining different materials, either through multimaterial printing^[1-6] or by directly incorporating different materials within a single filament.[7,8] Recently, additional functionalities have been imparted by using inks which themselves possess a hierarchical structure. Examples include foams or phase-separated resins for porous materials, [9–11] tunable viscoelastic polymers for mechanically graded materials,[12] self-assembled block copolymers to produce structurally colored materials,[13,14] and even extend to embedding bacteria or cells to create "living materials." [15,16] A promising class of materials that is yet to be fully explored for introducing functionality through complex nanostructuring

are liquid crystalline systems. To date these materials have only been used to create filaments with nematic alignment along the extrusion direction, [17-19] while more complex microstructures, such as the cholesteric phase, are not yet demonstrated. As an example, inks based on cellulose nanocrystals, which usually organize into a cholesteric phase within the bulk suspension, were reported to align upon extrusion to form a nematic phase.[19]

Cellulosic polymers are ideal candidates to introduce liquid crystalline ordering into 3D printing techniques. Not only are they a renewable resource, but they have also been demonstrated to organize into tunable cholesteric phases when dissolved in solution.[20-22] One such derivative, hydroxypropyl cellulose (HPC), is widely available and biocompatible. It selfassembles into a cholesteric phase in water, which can display vibrant, metallic structural colors that can be retained in the solid state via a variety of chemical and physical methods.^[22–27] However, the geometry of photonic HPC based materials has been so far limited to uniform or symmetrical geometries, such as thin films^[22–26] or cylindrical structures.^[27] Furthermore, as the resultant colors are often intrinsically linked to www.advancedsciencenews.com



www.afm-iournal.de

the processing conditions of the sample, current fabrication methods cannot be readily extended to other geometries. Therefore, in this study we applied a direct ink writing approach to the HPC mesophase to introduce a larger degree of geometric flexibility. Notably, while this approach has been previously used for HPC-based composite inks, [28,29] there have not been any studies that reported cholesteric ordering in the final object. Combined with the lyotropic properties of HPC, this allows for photonic structures to be designed with independent tunability over shape and color. In addition, with a feedstock consisting primarily of cellulosic polymers in water, using HPC as a photonic ink offers an environmentally friendly alternative to current 3D printable colored materials.

In this study, methacrylate-functionalized hydroxypropyl cellulose (HPC-MA) was combined with in situ UV crosslinking to produce filaments with an internal helicoidal nanoarchitecture, enabling the 3D printing of solid, volumetric objects with structural color. By investigating the shear-induced processes that determine the microstructure of the extruded material we show that the cholesteric mesophase is distorted and then aligned during extrusion. This understanding allows for a greater degree of control over the final structure both at the microscopic and macroscopic levels, while also unlocking the development of sustainable photonic filaments for 3D printing.

2. Results and Discussion

To combine the lyotropic liquid crystalline behavior of a cellulosic polymer with a photo-crosslinkable system, HPC was functionalized with methacrylic anhydride to yield "HPC-MA" in a single step (see Methods). As the liquid crystalline behavior of cellulosic polymers critically depends on the side chain chemistry, the effect of methacrylation upon the photonic architecture prior to printing was first verified. [20,30] When dissolved in aqueous solution, HPC-MA was found to form a cholesteric phase, but with an increased pitch relative to an equivalent HPC solution of the same concentration (e.g., at 64 wt% shown in Figure S1, Supporting Information). This pitch increase is likely an effect of introducing hydrophobic moieties, which was previously observed by Marsano et al. to amplify the effect of "water structuring" on the lyotropic behavior resulting in the cholesteric phase forming at lower concentrations.^[31] Furthermore, upon increasing the degree of methacrylation (DMA, the ratio of methacrylated groups to anhydroglucose units), a redshift in the reflected color was also observed for HPC-MA (Figure S1, Supporting Information). The DMA can be determined from ¹H-NMR spectroscopy (Section S1 and Figures S2-S4, Supporting Information), with a range of 0.10-0.12 selected for all printing inks used in this work (equivalent to approximately 3-5% of hydroxyl groups being functionalized along the HPC chain). This relatively high degree of substitution allows for a high crosslinking density as well as fast crosslinking kinetics, which should prevent distortion or disruption of the photonic nanoarchitecture upon subsequent solvent loss or manipulation.

An aqueous HPC-MA mesophase (64 wt%) was selected as an ink to 3D print photonic structures. At this concentration, the loss modulus G'' of the HPC-MA mesophase always exceeds the storage modulus G' within the range of oscillatory

frequencies and amplitudes measured (Figure S5, Supporting Information). This suggests that in the printing process, during which the shear rates experienced at the nozzle walls are equivalent to a frequency range of 1-4900 rad s-1 (Section S2 and Figure S6, Supporting Information), the HPC-MA ink behaves like a viscous fluid with rate dependent viscosity. With a displacement-driven extrusion printing mechanism used in our 3D printing platform, the mesophase is able to flow during and after nozzle extrusion, upon which the shape of the extruded ink can be fixed using photo-crosslinking. To print complex structures spanning several layers in height, the gelation of the mesophase was induced by photo-crosslinking the pendant methacrylate groups in situ. By coupling an ultraviolet (UV) light source ($\lambda_{\text{max}} = 365 \text{ nm}$, $E_{\text{max,av}} = 4.6 \text{ mW cm}^{-2}$ as calculated in Figure S7, Supporting Information) to the printing setup (Figure 1a), HPC-MA could be continuously crosslinked during deposition. With this UV irradiance, the gelation time, which is defined here as the time required for the storage modulus G' to exceed the loss modulus G'' for a defined shear frequency and amplitude, was estimated to be below 30 s by irradiating HPC-MA in situ during a rheometer measurement (Figure S8, Supporting Information). Such a gelation time allowed for the cumulative build-up of printed layers with good control of the structure and inter-filament integration, as exemplified in Figure 1b,c, although it did not allow for overhanging structures. While the rheological properties could be tuned to allow overhanging structures by including modifiers, [28,29,32] significant changes to the ink's rheological properties could affect the ability to retain the structural color after printing. In addition, a more focused UV source might allow even faster crosslinking and consequently, reduced flow prior to gelation; however, this could compromise the integration between subsequently printed filaments. It should be noted that the 3D-printed objects are shown encased in polydimethylsiloxane (PDMS) to allow the structural coloration to be assessed in the absence of surface scattering (Section S3 and Figures S9-S11, Supporting Information).

The color of most 3D-printed objects depends primarily on the chemical structure of the pigment or dye included within the filaments. In contrast, the color of the lyotropic HPC-MA mesophase is determined by the periodicity (or pitch) of the cholesteric ordering, which varies according to its concentration.^[21] As such, mesophases with different colors can be prepared by changing the ratio of HPC-MA and water. By crosslinking and subsequently drying, solid films capable of reflecting across the entire visible spectrum could be prepared (**Figure 2a**,b).

The color change arising from UV-crosslinking and the subsequent loss of water is a complex process. A redshift is observed as an HPC-MA solution is exposed to UV irradiation (as shown in Figure 2c). This redshift is attributed to small increases in temperature as the cholesteric HPC-MA solution is thermochromic and redshifts with increasing temperature.^[33] While UV absorption and heating due to irradiation could contribute in part to this redshift (as observed for unfunctionalized HPC in Figure S12, Supporting Information), the majority of the temperature change is likely from the enthalpy of reaction as the polymerization of methacrylate groups is typically exothermic.^[34] This was confirmed by the fact that the shift in color is dependent on the reaction rate: increasing the reaction rate

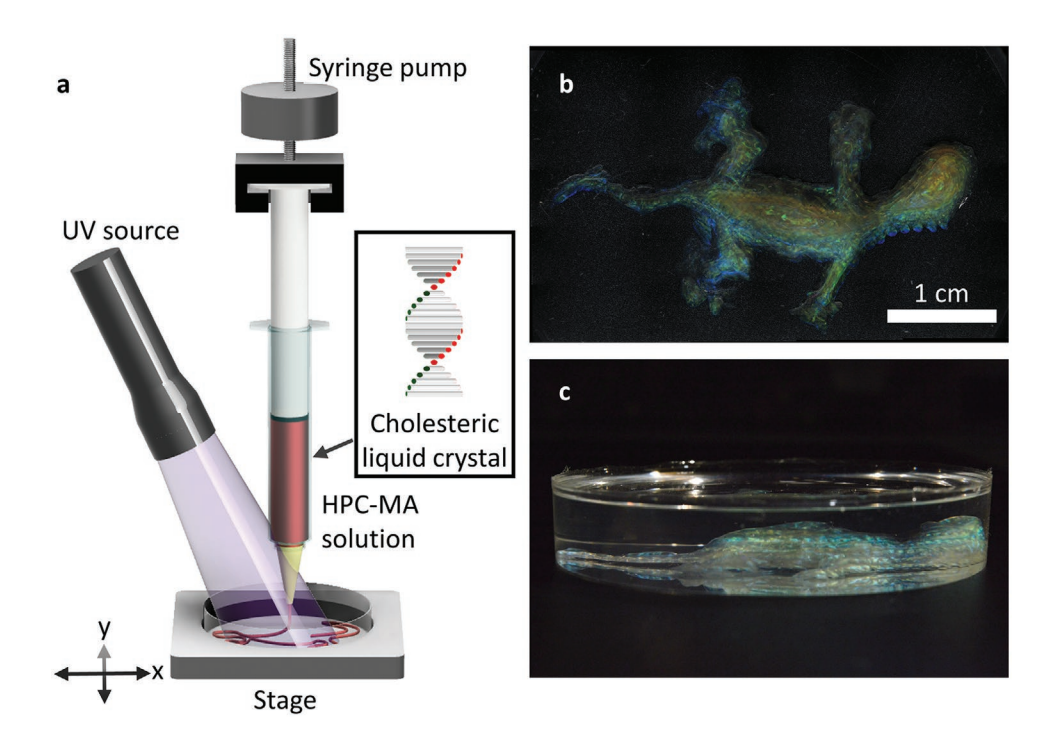


Figure 1. a) Schematic of the direct-write 3D printing setup with in situ UV crosslinking, the inset represents the structure of a cholesteric liquid crystal formed by HPC-MA. A 3D-printed "gecko" with structural color produced from an initial concentration of 64 wt% HPC-MA, as viewed from b) the top (using a digital microscope) and c) side (using a camera). The object is encapsulated in polydimethylsiloxane to remove interfacial scattering.

by changing the power of the UV irradiation or the degree of methacrylation led to a larger redshift (Figure S13, Supporting Information).

After crosslinking, water evaporation from the mesophase results in volumetric contraction and a corresponding blueshift in the reflected color. The extent of the blueshift depends on the starting concentration of the HPC-MA solution (Figure S14, Supporting Information), with the degree of shrinkage proportional to the volume fraction of water that is lost. The consequence is that visible color can be observed in dried samples from a wide range of initial concentrations (Figure 2d), allowing for the color of a printed structure to be readily tuned by changing the concentration of the HPC-MA feedstock (Figure S15, Supporting Information).

The visual appearance of a cholesteric mesophase is not solely dependent on the length of the cholesteric pitch, but also on the arrangement and alignment of individual domains.^[24] Here, the printed object, which is formed from an assemblage of printed HPC-MA filaments, possesses a different appearance compared to a bulk film cast from the same solution. As such, to understand how the extrusion and drying processes affect the final microstructure, the nanoscale ordering of printed filaments was examined by scanning electron microscopy (SEM). The filaments within a model structure that consisted of a three layer "staircase" were imaged in cross section, as shown in Figure 3a-f and Figure S16 (Supporting Information). The approximate contours of a single filament are highlighted by the black dotted outline in Figure 3b, which show a deformation from the circular cross-section at the exit of the nozzle due to flow prior to gelation. The periodic fracture planes characteristic of a cholesteric structure can be observed under higher

magnification, which crucially indicates that the liquid crystalline ordering is retained in the printed structure. Notably, these fracture planes follow the contours of the filament, although a disordered central region is observed in some cases (Figure 3c,e). As the initial HPC-MA mesophase is polydomain, this was attributed to the ordering that arises during the shear applied during extrusion. This complex architecture is responsible for the highly angular dependent character of the printed structure, with a strong blueshift observed for higher angles of incident light (Figure S17, Supporting Information).

To understand the behavior of HPC-MA solution under extrusion, the shear rate experienced within the nozzle was examined. As the rheological behavior of HPC is time-dependent, the duration under shear was also considered (i.e., the "residence time" in the nozzle). [35] This is important as previous studies of cholesteric, albeit colloidal, systems have indicated that shear alignment is localized to the nozzle wall if insufficient time is provided. [19] Here, both the shear profile at the nozzle wall and the residence time can be estimated by assuming a plane Poiseuille flow, [36] thus approximating the shear experienced by the mesophase near the interfaces of the channel (Section S2 and Figure S6, Supporting Information).

The estimated wall shear rate and how this affects the cholesteric microstructure was considered within the context of the rheological response of HPC-MA. In a cone/plate rheometer, HPC-MA retains the characteristic behavior of an HPC mesophase under shear, which typically exhibits three shear thinning regimes (Figure S5, Supporting Information). [35–38] For the high shear regime, estimated here to be above a critical shear rate at approximately 1 s⁻¹ for a 64 wt% HPC-MA solution, the cholesteric liquid crystal is reported to form a shear aligned state,

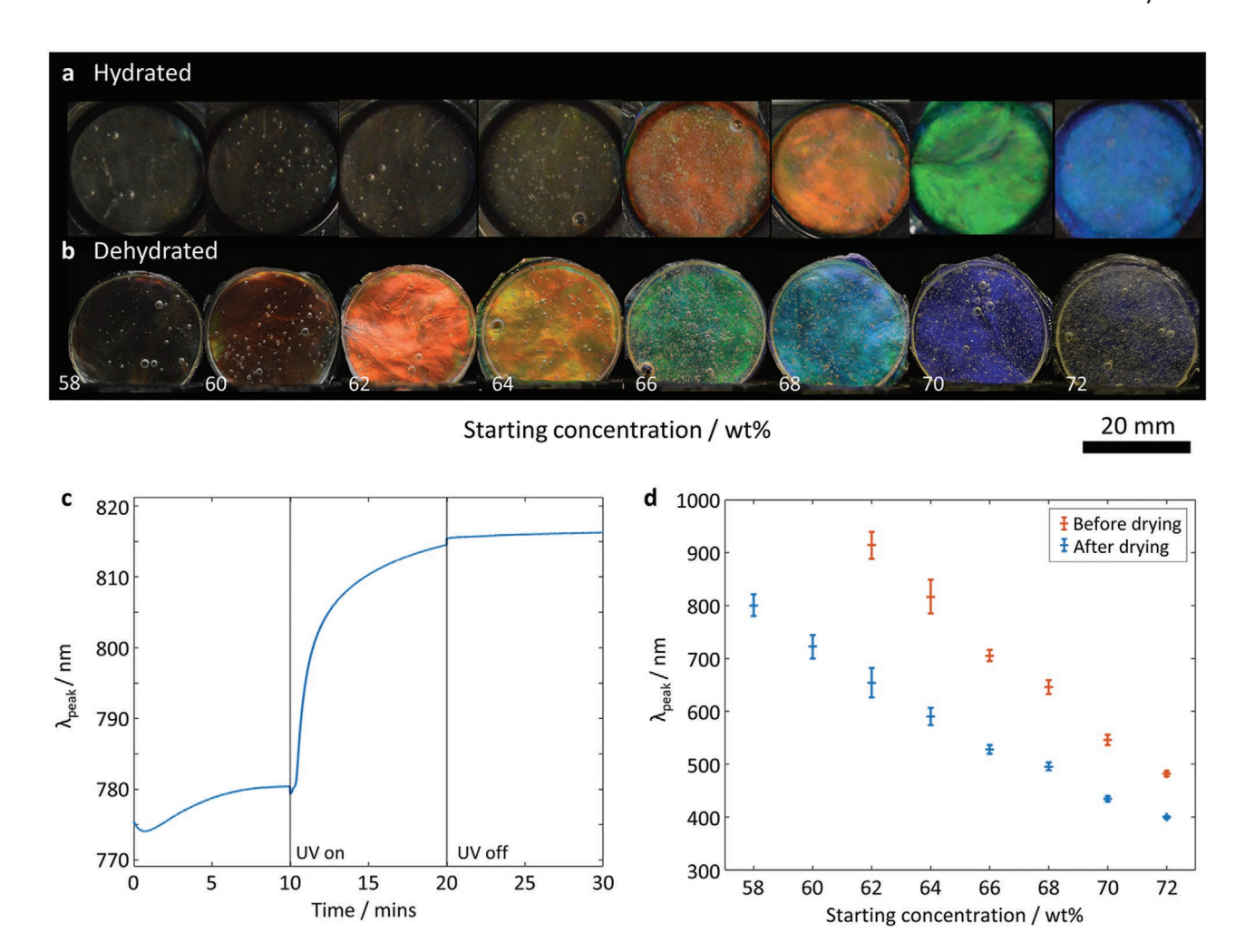


Figure 2. Photographs of aqueous HPC-MA mesophases with increasing concentration recorded a) after UV crosslinking and b) after subsequent loss of water to form a freestanding film. c) Plot showing the change in the peak reflected wavelength λ_{peak} of a 64 wt% HPC-MA solution during the photo-crosslinking process. The time points at which the UV source was turned on and off are indicated by the black lines. d) Average peak reflected wavelength λ_{peak} of HPC-MA films with different initial concentrations after UV irradiation (red points) and complete water loss (blue points). Each point represents an average of 15 spectra with the standard deviation represented by the error bars. The peak reflected wavelengths prior to drying for 58 and 60 wt% extend into the infrared region, and as such are outside the detection range of the spectrometer.

resulting in a nematic-like aligned arrangement of polymer chains that is associated with a large rise in birefringence. A similar increase in birefringence is observed when an HPC mesophase was subject to a mixture of shear and extensional strains (slit contraction),[39] suggesting that under sufficient shear the polymer chains within the cholesteric phase would align in the shear direction. As the modeled shear rate toward the tip of the nozzle far exceeds the critical shear rate required for alignment, one might conclude that the complete shear alignment to give nematic ordering occurs within the nozzle and the cholesteric only reforms post extrusion. However, the restoration of a cholesteric structure from a shear aligned state is reportedly on the order of minutes, [40] which is far too long relative to the gelation time employed here and as such this conclusion is unlikely.

To account for the time-dependence of HPC-MA's rheological behavior, the estimated shear profile was directly replicated on a rheometer, either using a cone/plate or a parallel plate geometry (Figure S18, Supporting Information). In the latter

Adv. Funct. Mater. 2022, 2108566

configuration the visual appearance of the sample was monitored between crossed polarizers (Video S1 and Figures S19 and S20, Supporting Information). Although the color is difficult to interpret due to the convolution of color from the cholesteric structure (reflection and transmission) and the polymeric alignment (birefringence), the change remains indicative of the structural transformation during the shear process (see schematic in Figure S19, Supporting Information). At increasing shear rates, the color becomes increasingly cloudy and the colored stripes along the shear direction suggest an increase in birefringence, and accordingly, polymer alignment (Figure S20, Supporting Information). The color ultimately disappears at high shear (3:20 in Video S1, Supporting Information), which can be attributed to a large retardance and therefore a high order interference.[41] This indicates that there is a high degree of alignment after the application of the estimated shear profile.

To visualize the microstructure in this aligned state, the estimated shear profile was applied with a UV-coupled rheometer.

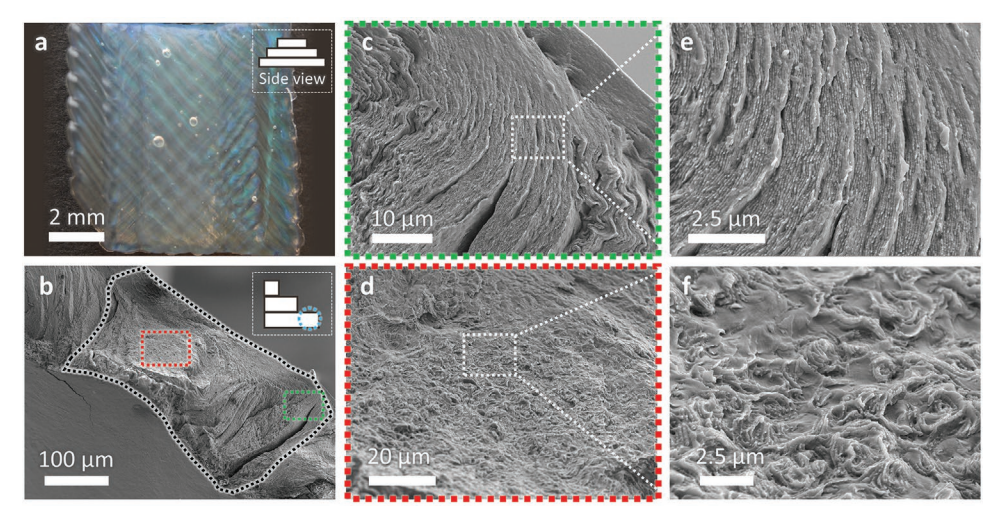


Figure 3. a) Photograph of a printed model three layer "staircase" structure produced from an initial concentration of 64 wt% HPC-MA with the inset showing a simplified schematic of the side view of the three layers. b) Cross-sectional SEM images of a constituent filament in (a), highlighting an ordered region near the edge (green box) and a more disordered region toward the core (red box). The inset represents the approximate position within (a) at which the SEM was recorded, and the approximate interface of the constituent filament is indicated as the black dotted line. c,d) Cross-sectional SEM images of the regions indicated by the green and red boxes in (b). e,f) Cross-sectional SEM images at a higher magnification of (c,d), demonstrating the characteristic fracture planes of the ordered and disordered regions.

In this case, the sheared plate was crosslinked in situ immediately after the application of shear, resulting in no color being observed, except for a small region at the center of the plate (Figure S21, Supporting Information). This is consistent with the radially increasing shear rate expected for a parallel plate geometry. Examination of the microstructure via SEM within the noncolored region revealed a highly disordered structure with some regions resembling that of cholesteric ordering (Figure S22, Supporting Information), although this is complicated by the buckling observed throughout the sample and a large apparent pitch (>1 µm). This larger pitch could be a result of the "unwinding" effect of shear, as predicted for certain combinations of cholesteric orientation and shear directions.[42,43] Therefore, these observations suggest that while the applied shear rate does exceed that of the critical shear rate typically required to align HPC-MA, the short shear duration means that the cholesteric structure is disrupted rather than completely destroyed. Notably, when the sample was cross-sectioned along the shear direction, the fractured region displayed a fibrillar texture (Figure S22, Supporting Information). Such texture, which has been observed previously in sheared HPC mesophases, [44,45] can also be observed to a lesser extent in the printed structures (Figure S23, Supporting Information).

Following these observations, we therefore propose a mechanism to account for both the retention of the cholesteric structure and the alignment of the domains. Under shear, the cholesteric ordering is distorted and the procession of the director along the helicoidal axis more closely resembles a square wave rather than the typical sinusoidal depiction, [43,46] in which the majority of polymer chains become aligned toward the shear direction. In addition, the helical axis rotates, lying within a plane oblique to the shear direction. This plane is defined by a characteristic tilt angle θ_{tilt} that, in turn, is dependent on the shear applied (Figure 4a). [47] Such imposition of an overall average tilt increases the effective angle of incident light, which in addition to any distortions to the cholesteric

pitch, results in a visible blueshift (Video S2 and Figure S24, Supporting Information).^[48]

The distortion-induced alignment mechanism, coupled with surface anchoring effects, [43] can, therefore, explain the observed microstructure in the printed filaments. As shown schematically in Figure 4c, the mesophase is initially polydomain at the top of the nozzle, but as the material is extruded, shear-induced helical axis rotation within the nozzle causes the helical axes of each domain to become increasingly aligned and tend toward a fixed angle relative to the nozzle wall. The resultant blueshift increases in magnitude toward the tip of the nozzle as the shear rate increases (Figure 4b and Video S3, Supporting Information). Once the filament is extruded, the helical axes of the cholesteric domains remain radially oriented, as there is little time for reorganization of the microstructure within the timescale of the UV-crosslinking process.

The fixed domain alignment upon exit from the nozzle was verified by printing a filament that was crosslinked only after it had been fully extruded (Figure S25, Supporting Information). While the region closest to the nozzle experienced only a minimal relaxation time, the microstructure is comparable to that of a region that had been allowed to relax over a longer period (Figure S26, Supporting Information). In terms of visual appearance, an increased relaxation time results in a small redshift, which indicates a relaxation of the mesophase. Macroscopically, these filaments can also be observed to become wider and more deformed due to lateral flow under gravity when compared to those that have been continuously crosslinked. Similar effects are observed when filaments printed with different gauge nozzles, leading to different filament widths (Table S1, Supporting Information), are compared. At small gauge sizes (i.e., a larger nozzle diameter), a region of disordered domains can be observed at the core, as exemplified for filaments printed using a nozzle with an outlet inner diameter (ID) of 0.25 mm in Figure S27 (Supporting Information). In comparison, such a region was not observed for those www.advancedsciencenews.com www.afm-journal.de

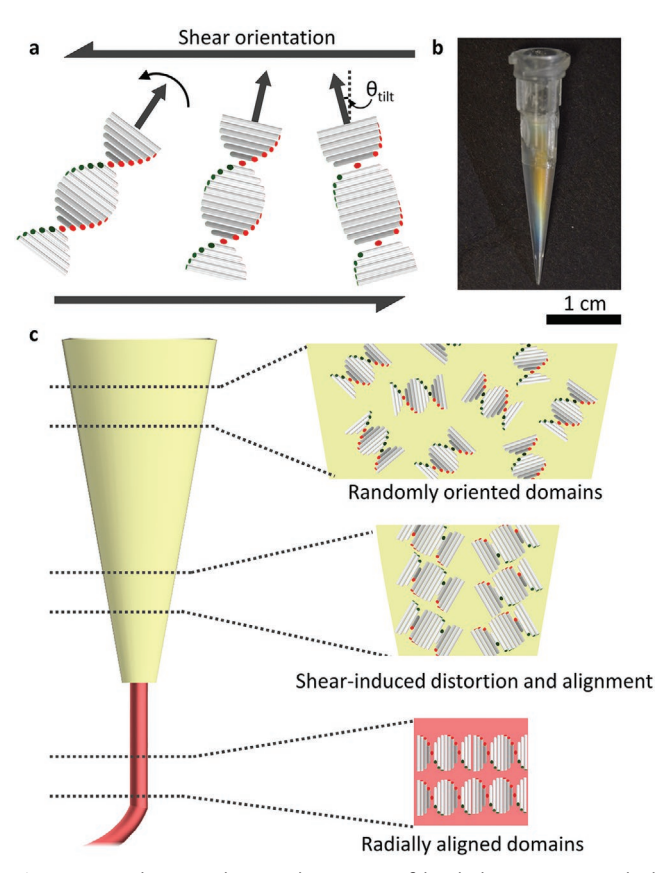


Figure 4. a) Schematic showing the rotation of the cholesteric axis (marked as a black arrow) when under shear (orientation shown by the two half arrows). The characteristic domain tilt (measured relative to the normal of the shear orientation) for the given shear process is shown by $\theta_{\rm tilt}$. b) Photograph of a transparent nozzle containing 64 wt% HPC-MA, which has been crosslinked during the printing process. c) Schematic showing how the domain alignment and distribution evolves within the nozzle such that the extruded HPC-MA filaments have radially aligned domains.

printed using narrower nozzles (ID = 0.20 and 0.15 mm). This observation suggests that the orientating effects of wall shear arising from extrusion through the nozzle are limited in range and weaken toward the core of the filament.

The thermochromicity of HPC mesophases^[22,25,33] offers an additional flexibility toward in situ tuning of the structural color of the 3D-printed object. The HPC-MA mesophase demonstrates a strong redshift upon heating, with a 70 wt% solution shifting from blue to red upon mild heating from 22 to 30 °C. While this thermochromic effect is typically reversible, crosslinking traps the liquid crystalline organization, preventing any recovery as the temperature is lowered. This property was exploited to yield films with different colors using the same initial feedstock, as shown in Figure 5a-d. In addition, this thermochromic behavior allowed for the multicolor printing of simple designs from a single HPC-MA feedstock (Figure 5e) in two steps, i.e., a 3D printing followed by crosslinking at elevated temperature. Printing at room temperature avoids challenges associated with changes in viscosity at higher temperatures (Figure S28, Supporting Information), which would have necessitated a different set of printing and crosslinking parameters. Furthermore, by maintaining a high humidity environment while the material was heated and subsequently crosslinked, drying during this process was successfully inhibited, which allowed for precise control over the final color and shape.

3. Conclusions

In summary, an aqueous solution of methacrylate-functionalized hydroxypropyl cellulose was used as a sustainable, green and nontoxic feedstock for additive manufacturing. By combining this material with an in situ UV crosslinking approach, 3D-printed cellulosic objects with predefined structural colors were produced. While there is a trade-off between print resolution and the intensity of the reflected color, the printed system offers independent control over the visual appearance and structure. Furthermore, owing to the thermochromic behavior of liquid crystalline HPC, objects with different colors could be produced by simply changing the crosslinking temperature post printing, opening up the opportunity to print different colors using the same feedstock. Finally, by examining the microstructure of the printed filaments as well as the rheological behavior of the mesophase, a mechanism has been proposed to account for the well-aligned microstructure after the print process, which opens a pathway toward the 3D printing of a wide variety of cholesteric liquid crystal systems.

4. Experimental Section

Synthesis of HPC-MA: Dry hydroxypropyl cellulose powder (HPC SSL SFP, food grade, $M_{\rm w}=40000~{\rm g~mol^{-1}}$ as reported by manufacturer) was purchased from Nisso Chemical Europe, and dried under vacuum overnight prior to use.

Methacrylic anhydride and 2-hydroxy-4'-(2-hydroxyethoxy)-2-methylpropiophenone were purchased from Sigma Aldrich and used as supplied without further purification.

The HPC-MA synthesis was adapted from a protocol for methacrylated hyaluronic acid.^[49] A solution of dried HPC powder (10.0 g) in water (500 mL) was prepared, to which methacrylic anhydride (40 mL) was added. Sodium hydroxide (5N, 59 mL) was then added dropwise over 30 min, prior to the reaction mixture being left to stir overnight at room temperature. The opaque white mixture was then dialyzed against water for at least 3 d before being lyophilized to yield HPC-MA as loose white flakes. Typically, prior to lyophilization, 3–4 batches were combined for ease of processing to produce a larger quantity of polymer. The average yield by polymer mass is 75 wt%.

Formulation of HPC-MA: HPC-MA polymer was dried under vacuum overnight prior to sample preparation. In order to produce 10 g of 66 wt% HPC-MA solution, 3.4 g of water was added to 6.6 g of polymer, and the mixture was immediately mixed using a planetary mixer (Thinky ARE-250, with THI250AD-201 adaptor and THI150ML container). Subsequently, 2-hydroxy-4'-(2-hydroxyethoxy)-2-methylpropiophenone (66 mg, 1 wt% relative to HPC-MA) was added and the formulation was mixed a second time. The formulation was then degassed by centrifuging at 5000 g (Thermofisher Heraeus Multifuge X1R, with a Thermofisher Fiberlite F15 rotor). The duration of the centrifugation step depended on the application of the solution, from 30 min for optical characterization to 2 h for rheological and printing applications. Samples of different starting concentration and total mass were prepared using an analogous method.

To prepare samples for optical characterization, HPC-MA solution was encapsulated between two parallel glass microscope slides separated by a rubber O-ring with a thickness of 2 mm. To reduce the effect of sample

www.advancedsciencenews.com

www.afm-journal.de

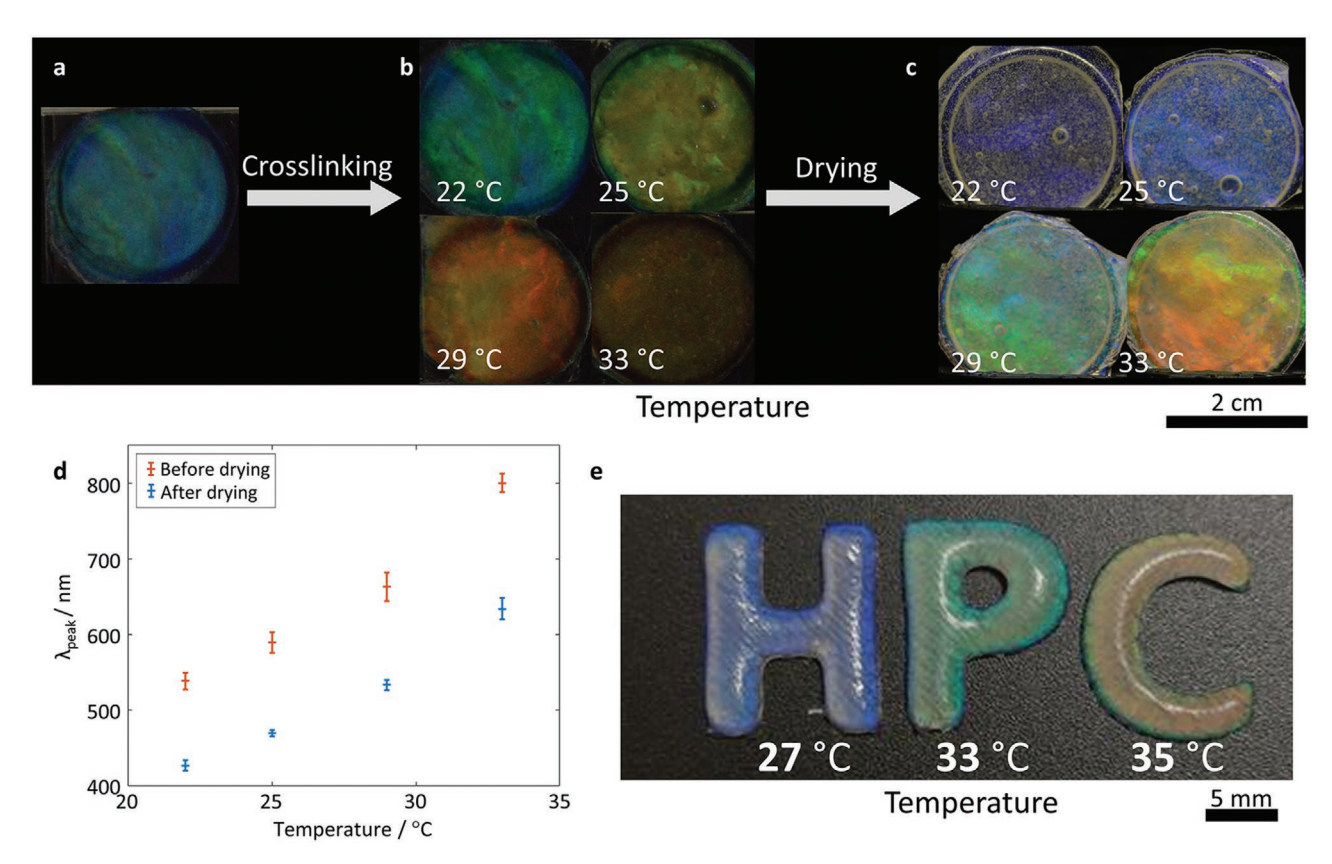


Figure 5. Photographs of a 70 wt% HPC-MA solution a) at rest at room temperature, b) after crosslinking at different temperatures, and c) after drying, showing the strong redshift with increasing crosslinking temperature. The temperature recorded is taken as an average over the crosslinking duration and measured on the top surface of the sample. d) Average peak reflected wavelength λ_{peak} of HPC-MA films crosslinked at different temperatures, as measured after UV irradiation (*red points*) and after subsequent water loss (*blue points*). Each point represents an average of five spectra with the standard deviation represented by the error bars. e) Photographs of 3D-printed letters: "H", "P", "C" produced from a single 68 wt% HPC-MA solution, but crosslinked at temperatures of 27, 33, and 35 °C, respectively.

preparation and self-assembly kinetics on the optical measurements, each sample was prepared at least 10 min prior to analysis, to allow for equilibration and relaxation. To measure the temperature dependence of the reflected color, the sample was additionally heat treated in a container inside an oil bath for at least 10 min prior to UV-crosslinking for a further 10 mins (schematic drawn in Figure S29, Supporting Information). The temperature was recorded using a thermocouple (Thorlabs TSP01) placed on the top surface of the sample and averaged over the duration of the crosslinking. The sample temperatures of 22, 25, 29, and 33 °C correspond, respectively, to oil bath temperatures of 22 (room temperature), 30, 40, and 50 °C (Figure S30, Supporting Information).

Printing of HPC-MA: All 3D-printed samples of HPC-MA were fabricated with a laboratory-built robotic bioprinter, as schematically shown in Figure 1c. The 3D STL files of the printed structures were downloaded from Thingiverse (www.thingiverse.com) ("All Alphabet Letters" by 6brueder; "Gecko" by Jbecerra). Prior to the printing process, the 3D CAD files of the printed structures were converted to G-code using a slicing software (Slic3r, https://slic3r.org/). The printing parameters of the samples fabricated in this study can be found in Table S2 (Supporting Information). HPC-MA solutions (64 or 68 wt% HPC) were used as the printing ink, which was drawn into a 1 mL syringe and was loaded into the syringe holder of the printer. The 3D structure was printed onto the surface of the petri dish by executing the G-code instructions. The "gecko" and "staircase" samples were crosslinked in situ during printing with an UV LED placed approximately 11 cm away from the stage (irradiance profile of the UV source during the printing process can be found in Figure S7 (Supporting Information), and the average peak irradiance $E_{\text{max,av}}$ is calculated to be 4.6 mW cm⁻²). They

were then further crosslinked using the same UV light source for 10 min after printing to ensure complete crosslinking. To maintain a humid environment during heating and crosslinking of the "letters" samples, they were warmed in an incubator (Thermo Scientific Midi CO_2 incubator) for 10 min after printing, followed by UV crosslinking for 10 min.

Characterization: Reflection spectra were obtained using a double-ended probe (Ocean Insight R200-7-SR) positioned below the sample, using a broadband light source (Thorlabs SLS201L/M) coupled to a spectrometer (Avantes AvaSpec-HS2048). The spectra were measured relative to a glass slide placed in front of a white diffuser (Labsphere SRS-99-010). For samples prior to UV crosslinking, a longpass filter with a cut-on wavelength of 400 nm (Thorlabs FELH0400) was additionally placed in the light path. In order to measure the effect of UV crosslinking, a UV LED (LED ENGIN LZ1-00UV00; $\lambda_{max} = 365$ nm) was directed from the top of the sample. A schematic of this setup is depicted in Figure S29 (Supporting Information) and the time-dependent irradiance of the UV source at difference substrate distances is represented in Figures S31 and S32 (Supporting Information).

Scanning electron microscopy was performed on a TESCAN MIRA3 FEG-SEM system at 5.0 kV. Cross-sectional samples were fractured under liquid nitrogen and sputter coated with Pt (10nm; Quorum Technologies Q150T ES) prior to measurement.

Rheometry was performed on an Anton Paar MCR302 Rheo-Microscope for the optical rheometry measurements and a TA Instruments Discovery HR-2 rheometer for all other measurements. Flow and temperature sweeps were conducted using a cone-plane geometry (20 mm, 1.0°) with a truncation gap of 28 μm. Prior to each flow sweep,



www.advancedsciencenews.com www.afr

_____ /MATERIALS
www.afm-iournal.de

the sample was sheared at a rate of 0.01 s⁻¹ for 30 min to allow the system to approach equilibrium. The flow sweeps were conducted at 20 °C. UV-coupled rheometer measurements, amplitude, and frequency sweeps were conducted using a parallel plate geometry (20 mm) with a gap of 1000 μm . The UV light source for rheometry measurements was supplied by a Omnicure S2000 Spot UV curing system. The optical rheometry measurements were taken using a parallel plate geometry (25 mm) with a gap of 1000 μm at 25 °C and observed in reflection using a 5× objective (Mitutoyo M Plan Appo 5x) between crossed polarizers (schematic shown in Figure S19, Supporting Information).

Supporting Information

Supporting Information is available from the Wiley Online Library or from the author.

Acknowledgements

This work was funded by a BBSRC David Phillips fellowship (BB/K014617/1) to S.V.; by a Croucher Cambridge International Scholarship to C.L.C.C.; by ERC (ERC-2014-STG H2020 639088) to C.L.C.C., R.M.P., and S.V.; by ERC (ERC-2017-POC 790518) to R.M.P. and S.V.; by ERC (ERC-2020-POC 963872) to S.V. and C.L.C.C.; by ERC (ERC-StG, 758865) to. Y.Y.S.H.; by EPSRC (EP/R513180/1) to K.D.R. and R.C.E.; by the EU Horizon 2020 research and innovation programme under the Marie Skodowska-Curie grant agreement (722842: ITN Plant-inspired Materials and Surfaces - PlaMatSu) to G.T.K.; by a WD Armstrong Trust Studentship and a Macao Postgraduate Scholarship to I.M.L. The authors thank Dr. Renata Sala for guidance on the rheological measurement, Dr. Harry Ayton for guidance on the shear rate modeling, Dr. Bruno Frka-Petesic for helpful discussions on liquid crystalline systems under shear, Dr. Johannes Haataja for useful discussions on electron imaging, and Dr. Karin Müller from the Cambridge Advanced Imaging Centre.

Conflict of Interest

The authors declare no conflict of interest.

Data Availability Statement

The data that support the findings of this study are openly available in University of Cambridge data repository at https://doi.org/10.17863/CAM 72193

Keywords

Adv. Funct. Mater. 2022, 2108566

3D printing, hydroxypropyl cellulose, liquid crystals, structural color, sustainability

Received: November 8, 2021 Published online:

- [1] D. Kokkinis, M. Schaffner, A. R. Studart, Nat. Commun. 2015, 6, 8643.
- [2] L. Alison, S. Menasce, F. Bouville, E. Tervoort, I. Mattich, A. Ofner, A. R. Studart, Sci. Rep. 2019, 9, 409.
- [3] M. Schaffner, J. A. Faber, L. Pianegonda, P. A. Rühs, F. Coulter, A. R. Studart, Nat. Commun. 2018, 9, 878.

- [4] D. Kokkinis, F. Bouville, A. R. Studart, Adv. Mater. 2018, 30, 1705808.
- [5] F. B. Coulter, M. Schaffner, J. A. Faber, A. Rafsanjani, R. Smith, H. Appa, P. Zilla, D. Bezuidenhout, A. R. Studart, *Matter* 2019, 1, 266
- [6] E. L. Gill, X. Li, M. A. Birch, Y. Y. S. Huang, Bio-Design Manuf. 2018, 1, 77.
- [7] G. Loke, R. Yuan, M. Rein, T. Khudiyev, Y. Jain, J. Joannopoulos, Y. Fink, Nat. Commun. 2019, 10, 4010.
- [8] W. Wang, K. Ouaras, A. L. Rutz, X. Li, M. Gerigk, T. E. Naegele, G. G. Malliaras, Y. Y. S. Huang, Sci. Adv. 2020, 6, eaba0931.
- [9] D. G. Moore, L. Barbera, K. Masania, A. R. Studart, *Nat. Mater.* 2020, 19, 212.
- [10] C. Minas, D. Carnelli, E. Tervoort, A. R. Studart, Adv. Mater. 2016, 28, 9993.
- [11] D. Zhang, P. Davoodi, X. Li, Y. Liu, W. Wang, Y. Y. S. Huang, Sci. Rep. 2020, 10, 18783.
- [12] P. A. G. S. Giachini, S. S. Gupta, W. Wang, D. Wood, M. Yunusa, E. Baharlou, M. Sitti, A. Menges, Sci. Adv. 2020, 6, eaay0929.
- [13] H. S. Kang, J. Lee, S. M. Cho, T. H. Park, M. J. Kim, C. Park, S. W. Lee, K. L. Kim, D. Y. Ryu, J. Huh, E. L. Thomas, C. Park, Adv. Mater. 2017, 29, 1700084.
- [14] B. B. Patel, D. J. Walsh, D. H. Kim, J. Kwok, B. Lee, D. Guironnet, Y. Diao, Sci. Adv. 2020, 6, eaaz7202.
- [15] M. Schaffner, P. A. Rühs, F. Coulter, S. Kilcher, A. R. Studart, Sci. Adv. 2017, 3, eaao6804.
- [16] M. Samandari, F. Alipanah, K. Majidzadeh-A, M. M. Alvarez, G. Trujillo-De Santiago, A. Tamayol, Appl. Phys. Rev. 2021, 8, 021404.
- [17] S. Gantenbein, K. Masania, W. Woigk, J. P. W. Sesseg, T. A. Tervoort, A. R. Studart, *Nature* 2018, 561, 226.
- [18] A. Sydney Gladman, E. A. Matsumoto, R. G. Nuzzo, L. Mahadevan, J. A. Lewis, Nat. Mater. 2016, 15, 413.
- [19] M. K. Hausmann, P. A. Rühs, G. Siqueira, J. Läuger, R. Libanori, T. Zimmermann, A. R. Studart, ACS Nano 2018, 12, 6926.
- [20] J. C. Thies, J. M. G. Cowie, Polymer 2001, 42, 1297.
- [21] R. S. Werbowyj, D. G. Gray, Macromolecules 1984, 17, 1512.
- [22] G. Maxein, M. Müller, R. Zentel, ACS Symp. Ser. 2001, 786, 61.
- [23] M. Müller, R. Zentel, Macromol. Chem. Phys. 2000, 201, 2055.
- [24] C. L. C. Chan, M. M. Bay, G. Jacucci, R. Vadrucci, C. A. Williams, G. T. de Kerkhof, R. M. Parker, K. Vynck, B. Frka-Petesic, S. Vignolini, Adv. Mater. 2019, 31, 1905151.
- [25] S. N. Bhadani, D. G. Gray, Mol. Cryst. Liq. Cryst. 1984, 102, 255.
- [26] S. Suto, S. Hasegawa, J. Mater. Sci. 2002, 37, 4857.
- [27] A. Thomas, M. Antonietti, Adv. Funct. Mater. 2003, 13, 763.
- [28] F. R. Gleuwitz, G. Sivasankarapillai, G. Siqueira, C. Friedrich, M.-P. G. Laborie, ACS Appl. Bio Mater. 2020, 3, 6049.
- [29] L. S. Ebers, M. P. Laborie, ACS Appl. Bio Mater. 2020, 3, 6897.
- [30] D. G. Gray, Carbohydr. Polym. 1994, 25, 277.
- [31] E. Marsano, E. Bianchi, S. Gagliardi, F. Ghioni, Polymer 2000, 41, 533.
- [32] C. H. Barty-King, C. L. C. Chan, R. M. Parker, M. M. Bay, R. Vadrucci, M. De Volder, S. Vignolini, Adv. Mater. 2021, 33, 2102112.
- [33] S. Fortin, G. Charlet, Macromolecules 1989, 22, 2286.
- [34] P. K. Mahato, D. Chanda, A. Borthakur, K. V. Rao, *Thermochim. Acta* 1993, 222, 265.
- [35] N. Grizzuti, S. Cavella, P. Cicarelli, J. Rheol. 1990, 34, 1293.
- [36] J. F. Steffe, Rheological Methods in Food Process Engineering, 2nd ed., Elsevier, East Lansing 1996.
- [37] T. Asada, K. Toda, S. Onogi, Mol. Cryst. Liq. Cryst. 1981, 68, 231.
- [38] K. Hongladarom, V. Secakusuma, W. R. Burghardt, J. Rheol. 1994, 38, 1505.
- [39] B. D. Bedford, W. R. Burghardt, J. Rheol. 1996, 40, 235.
- [40] Y. Geng, P. L. Almeida, G. M. Feio, J. L. Figueirinhas, M. H. Godinho, Macromolecules 2013, 46, 4296.



www.advancedsciencenews.com www.afm-journal.de

- [41] K. Hongladarom, W. R. Burghardt, Rheol. Acta 1998, 37, 46.
- [42] A. D. Rey, J. Nonnewton. Fluid Mech. 1996, 64, 207.
- [43] D. Marenduzzo, E. Orlandini, J. M. Yeomans, J. Chem. Phys. 2004, 121, 582.
- [44] Y. Nishio, T. Takahashi, J. Macromol. Sci., Part B 1984, 23, 483.
- [45] Y. Nishio, T. Yamane, T. Takahashi, J. Polym. Sci., Polym. Phys. Ed. 1985, 23, 1053.
- [46] J. H. Park, J. Noh, C. Schütz, G. Salazar-Alvarez, G. Scalia, L. Bergström, J. P. F. Lagerwall, ChemPhysChem 2014, 15, 1477.
- [47] J. M. Pochan, D. G. Marsh, J. Chem. Phys. 1972, 57, 1193.
- [48] D. F. Ciliberti, G. D. Dixon, L. C. Scala, *Mol. Cryst. Liq. Cryst.* 1973, 20, 27.
- [49] M. J. Rowland, C. C. Parkins, J. H. McAbee, A. K. Kolb, R. Hein, X. J. Loh, C. Watts, O. A. Scherman, *Biomaterials* 2018, 179, 199.

Adv. Funct. Mater. 2022, 2108566